Article

JOURNAL OF COMPOSITE MATERIALS

Journal of Composite Materials
2015, Vol. 49(21) 2557–2565

DOI: 10.1177/0021998314549821
jcm.sagepub.com
SAGE

Applicability of standard delamination tests (double cantilever beam and end notch flexure) for 5HS fabric-reinforced composites in weft-dominated surface

Marcos Yutaka Shiino[1], Reyndert Christiaan Alderliesten[2], Mauricio Vicente Donadon[3], Herman Jacobus Cornelis Voorwald[1] and Maria Odila Hilário Cioffi[1]

Abstract

Currently, the standard delamination tests established by ASTM (available for mode I and mix mode) are limited to unidirectional composites. Although some researchers have conducted delamination tests in woven composites, their information is still limited. In order to understand the propagation behavior and the value of fracture toughness of woven composites, this article evaluated a 5HS carbon/epoxy composite with a weft-dominated surface. Tests were conducted in double cantilever beam and end notch flexure configurations using an energy-based approach for data reduction in modes I and II, respectively. The results were assessed in terms of delamination resistance curves (R-curves). Both delamination modes showed consistent behaviors for extending the application of the standard procedures, as the energy variation can describe well the crack growth dependence of the irregular surface caused by the crimp, which was more pronounced for mode I.

Keywords

Fabrics/textiles, delamination, fracture toughness, laminate composites

Introduction

Fiber-reinforced polymer composites are known for their susceptibility to interlaminar ply delamination resulting in loss of stiffness or strength.[1,2] As a consequence, delamination in these materials under either quasi-static or fatigue loading has been the focus of many researches, in an attempt to develop improved damage tolerant materials.

The delamination resistance evaluation is usually based on the linear elastic fracture mechanics, and the most common approach for composites uses the energy balance introduced by Griffith. In this approach, the energy necessary for crack initiation is known as critical strain energy release rate (G_{Ic}), where the subscript I indicates the tensile or peeling opening mode.[3,4] The energy approach for crack propagation will be used to describe the studied cases of delamination in woven fabrics hereafter.

Some aspects that influence the measurement of G may arise from geometric and structural discontinuities.[5,6] An example of such influence was reported by Alif et al.[7] in woven glass and carbon composites that have a nonplanar structure. This type of structure interacts with the delamination propagation either at matrix or woven regions, where it has not been specified that whether it is in a weft or fill sections. Moreover, they did not observe the stick–slip behavior caused by the nonplanar structure, thus disagreeing with Ebeling et al.[6] who explained the influence based on crack-arresting behavior at the weft yarn (fiber tow perpendicular to crack propagation).

[1]Faculdade de Engenharia de Guaratinguetá, UNESP – Univ Estadual Paulista, Materials and Technology Department, Fatigue and Aeronautic Materials Research Group, Guaratinguetá-SP, Brasil
[2]Aerospace Structures & Materials, Faculty of Aerospace Engineering, Delft University of Technology – TUDelft, Delft, The Netherlands
[3]Instituto Tecnológico da Aeronáutica-ITA
Praça Marechal do Ar Eduardo Gomes, Vila das Acácias, São José dos Campos/SP, Brazil

Corresponding author:
Marcos Yutaka Shiino, UNESP Av. Dr. Ariberto Pereira da Cunha, 333 Guaratinguetá 12516-410, Brazil.
Email: marcosshiino@yahoo.com.br

Alif et al.[7] also defined the index n_g for the interlacing counting, 1 being for plain weave (PW), 2 for twill weave (TWILL) and $n_g > 2$ for harness satin (HS). The high index number is associated to a smaller degree of crack propagation constraint at the transverse yarns when the dominating surface is weft yarn parallel to the crack, and when observing it from the top.

Gill et al.[8] reported for all types of woven fabrics a steady-state plateau toughness being sharper for PW composites than for twill or satin weave due to its higher n_g index. The steady-state plateau toughness relates to the fiber bridging extension which is more pronounced for higher n_g values.

Hadavinia and Ghasemnejad[9] provided reasons for unstable crack propagation in mode I: intralaminar delamination; mixed-mode fracture; fiber bridging; micro-cracking; residual stresses. All these behaviors were observed in composites with $n_g = 2$, in which the R-curve presented unstable and stable crack propagation known as serrated profile shape. In the same reference, de R-curve for mode II propagation was presented without the serrated profile thus indicating less interference of the woven pattern.

De Baere et al.[10] also observed a serrated behavior in the load–displacement curve for a 5HS/PPS with decreasing load after reaching the nonlinear point (NL). The authors observed meta-delamination for this type of nonplanar structure, which indicates crack propagation in a plane above the symmetry plane. In respect to fracture toughness in mode II (G_{IIc}), they reported more stable initiation and also less scatter as compared to mode I.

In their investigation on the influence of fiber volume fraction (FVF) in mode II of 5HS/epoxy composite, Gill et al.[8] verified a preference of the crack path toward the upper arm in a new end notch flexure 4 (4ENF) set up, but did not present the reasons of different values found due to the variation in FVF.

Regarding the scatter in toughness values for mode II, most results were obtained for unidirectional composites. Schuecker and Davidson,[11] for example, found a value of $G_{IIc} = 1.2 \pm 0.35$ kJ/m^2 in 4-point bend ENF configuration resulting in 29% of coefficient of variation (CV) that is higher in comparison to values for mode I in a round robin tests conducted by ASTM D5528-01,[12] which also agrees with results found by Argüeles et al.[13] in unidirectional laminates. The high values of CV may relate to the method of crack onset detection that will be additionally discussed hereafter in a nonplanar surface.

Considering a brief review of some recent results, which mostly expressed fracture toughness values for unidirectional composites, this article investigated the possibility of extending the procedures of ASTM 5528-01 and the under-reviewed test standard method for mode II in a woven carbon fabric with a weft dominate surface, which had a symmetric architecture of 5HS/resin transfer molding 6 (RTM6) epoxy composite. The investigation gives a detailed description on the energy variation with delamination length and errors that may occur when delamination migrates to a different plane.

Materials and methods

Materials and process

The 5HS woven fabric supplied by HEXCEL was placed in a mold with dimensions of $300 \times 400 \times 3$ mm^3. The woven fabric had an aerial weight of 391 g/m^2, and consisted of 6 K tow carbon fibers with its surface coated by epoxy powder in order to result in a rectangular-shape preform. The resulting laminate with eight plies had a final FVF of about 58%. A 13-μm polytetrafluoroethylene insert film was introduced at the middle plane of the laminate to produce an artificial precrack, as specified in ASTM D5528-01.[12]

The laminate was produced via RTM using a bicomponent RTM-6 epoxy resin system also supplied by HEXCEL with a viscosity of 100 mPa s. The laminate was produced with a maximum injection pressure of 6 bar that took 80 min to fill the mold. The panel was subsequently cured at a temperature of 180°C for 120 min.

The final laminate was inspected with a through-transmission ultrasonic test with 1410 C-scan equipment. The 10 MHz probe scanned at 300 mm/s and moved 1 mm every each completed scan. The laminate plate presented good quality with an average and a minimum attenuation value of 23.54 ± 2.75 dB and 21.79 dB, respectively. A reference for rejection criteria in this plate was an average attenuation more than 28 dB attenuation that was based on some potential defects found in other batches.

Interlaminar fracture toughness

Quasi-static double cantilever beam (DCB) tests were carried out in accordance with the standard test method described in ASTM 5528-01[12] using an MTS testing machine with a 5 kN load capacity cell at room temperature. The mode I data reduction was conducted using modified beam theory (MBT). Further details of the data reduction are well outlined in ASTM D 5528-01.[12]

The tests were carried out under displacement control at a speed of 1 mm/min, and the onset of delamination was determined by visual identification of the precrack $\approx$ 2 mm (obtained by reload process) forward from the insert film to avoid any influence of the resin pocket created during the injection process.

The crack was monitored with a LINO lens of 50 mm diameter, 2.8 aperture, and the images were captured every 5 s with Labview v.12.0 software. These images were postprocessed with Image J software, which was also used to measure the resulting crack increments.

For mode II quasi-static tests, a similar specimen geometry was used but now loaded using a 3-point bending device. A support span was employed to be equal to $2L = 100$ mm, an initial crack length equal to $a_0 = 35$ mm, and a load nosing speed of 1 mm/min. The procedure was similar as adopted by O'Brien et al.[14] for unidirectional laminates. The data reduction procedures are presented in the Results and discussion section.

Results and discussion

Mode I – crack onset and propagation

Figure 1 shows the geometric patterns of a 5HS fractured surface tested in mode I. The dimensions of the fill and warp tows are $2 \times 7\,mm^2$ and $2 \times 2\,mm^2$, respectively.

According to ASTM D6856/D6856M-03(2008),[15] fill and warp tow are defined according to their construction. However, in this study, fill and warp tows were both used to keep the fiber tows at 90° ($T_{90°}$) to the crack propagation and also to make a symmetric laminate, in such a way to build a $T_{90°}$ dominated surface at the crack path. Thus, from now on, $T_{90°}$ is referred to tow perpendicular to the crack front and $T_{0°}$ is parallel to crack front.

For this specimen, a total crack length of 20 mm was considered for the propagation analysis. Most of the time the crack front, as indicated in orange dashed line in Figure 1, advanced through two or three $T_{90°}$ tows (same direction to the arrow, and in blue-dashed square) and two or three $T_{0°}$ tows widthwise, always in a 3:2 ratio.

As recommended by ASTM D5528-01 for the DCB tests, a first load cycle was performed in order to propagate the crack 1–2 mm ahead of the insert film, and then unloaded for the reload cycle to achieve the final crack length where it was measured G versus a.

The position of the insert film tip may influence the critical G_{Ic}, as it might point toward the neighboring layers, thus inducing the crack migration to other interfaces. This behavior differs from the unidirectional composites that might be considered when comparing the data scatter of both types of laminates. Another factor is the FVF that may constrain the crack tip. In case of high FVF, more scatter in results is observed in comparison to low FVF that has loose crack tip and toughness values approximates to the resin fracture toughness value.[8]

By following the crack progression from the composite's edge images as illustrated in Figure 2, which were also used to measure the G_{Ii} (index i indicates propagation), and comparing the fabric patterns in Figure 1, slow crack increment through the $T_{0°}$ tows was observed; afterwards the crack may not grow if it reaches a fill pattern or may experiment slow growth through a crack branching.

In case of crack tip arresting as illustrated in Figure 1 by square S, the accumulated elastic energy exceeds for a small increment (0.5 mm), and consequently a crack jump occurred, characterizing an unstable propagation. This statement is supported by

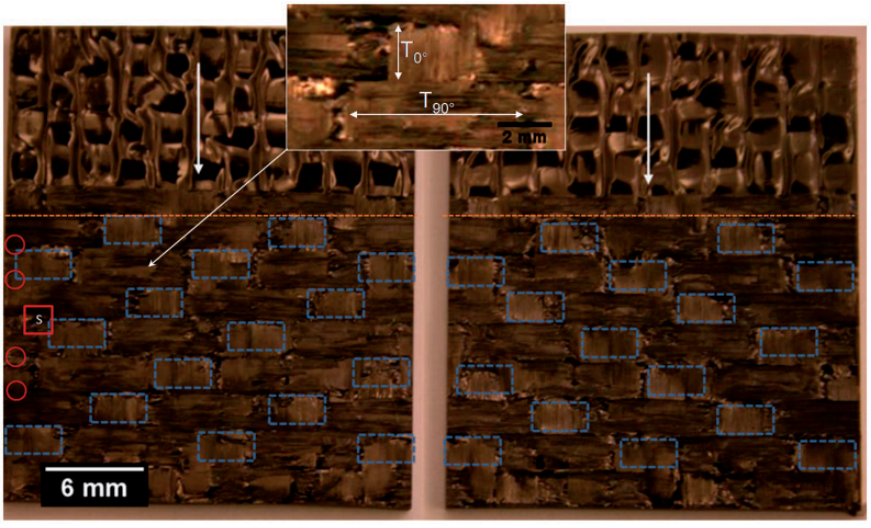

Figure 1. Coupon CP1 split into top (on left) and bottom.

the larger crack length and also a decrease in G value that is discussed in an R-curve later. In all T_{0° or T_{90° sections, there is no preference of branching as was observed in cross-ply composites.[16]

The crack progression observed here indicated a similar process as described by Ebeling et al.[6] for toughened resin systems with woven fabrics, which presented smooth growth through the T_{0° section followed by a jump through the T_{90° tow.

When observing the T_{90° tow from the free edge, what occurred was a crack arrest, Figure 1(a), but with smooth propagation through the T_{0° yarn according to Ebeling, and it will eventually overcome the next row of tows.

The 5HS composite in the studied fiber architecture has an area ratio of $A_{T_{90^\circ}}/A_{T_{0^\circ}} = 3.5$, which comprised predominantly T_{90° tow that substantially increased the energy at this section, and hence allowed just small crack advancement which was followed by unstable crack propagation. Therefore, the observed rate of crack propagation will be different from an area ratio of $A_{T_{0^\circ}}/A_{T_{90^\circ}} = 1$ of a PW composite that may show less energy accumulation in the T_{90° tow section.

The MBT was used for the data reduction on mode I. The linear fit to obtain the crack length correction (Δ) is shown in Figure 3. This method showed the most conservative value compared to compliance calibration and modified compliance calibration according to ASTM.[12]

The R-curve of G_{Ii} , where i means propagation, is shown in Figure 4. The first point of each curve is related to the crack onset (G_{Ic}). The arresting crack location corresponds to the highest peak of each R-curve. Before reaching the highest peak, the crack developed into small crack increments through the T_{0° tow, and consequently accumulating energy for a crack jump.

As reported previously, the energy accumulation might lead to unstable crack propagation greater than a single fiber tow (2 mm). For coupon 2 (CP2), two

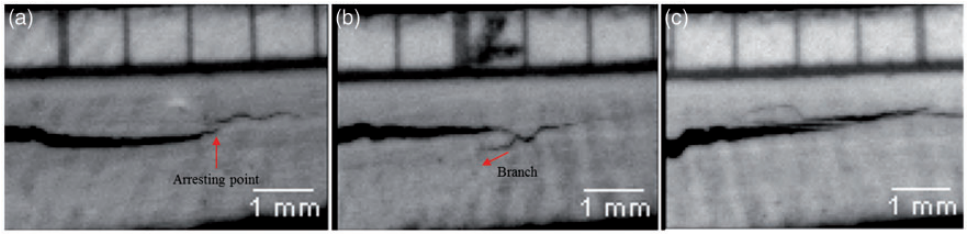

Figure 2. Detailed crack branches of coupon CP1 at: (a) 2 mm length, (b) half of the total length, and (c) the end.

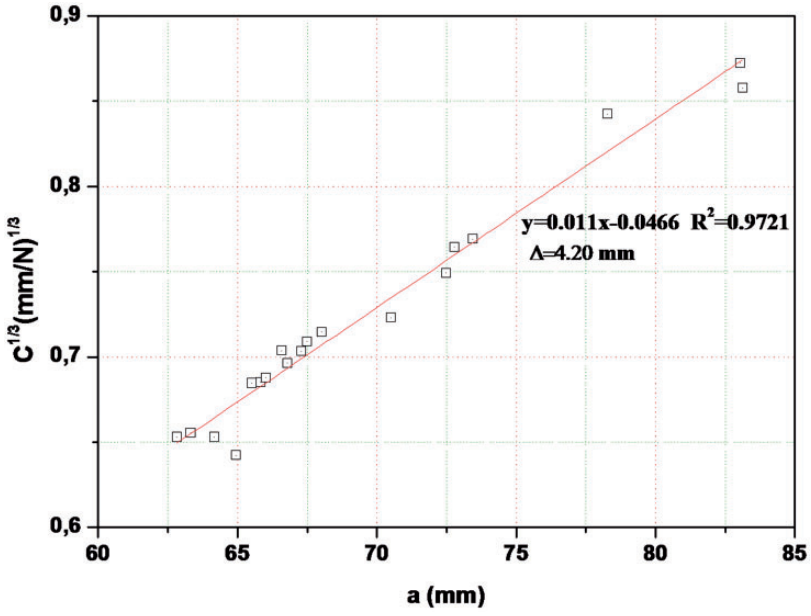

Figure 3. Linear fit for crack length correction in mode I.

unstable crack propagations occurred: the first one had energy to overcome a row of fiber tows and another accounted for two rows of fiber tows, as illustrated in Figure 4. Other coupons in Figure 4 followed a similar delamination pattern being the unstable crack propagation of two tows either close to the crack onset (a_0) or when it reached the very end of the delamination.

On the analysis of these five coupons, one characteristic feature that controlled the amount of energy for an unstable delamination process is the number of branches. In the observation of the crack length measurement for these coupons, the process of crack branching released the energy around the main crack prior to jump to the next row of tows, an investigation that was based on the comparison of CP1 to the other coupons, thus leading to smaller crack jump.

Despite the fact that this fabric presented less waviness than a PW fabric studied by Ebeling et al.,[6] the fracture toughness value for crack propagation is also controlled by fabric nonplanar features. This is exemplified with a lower net resin fracture toughness $G_{Ic} = 168$ J/m^2, HEXFLOW,[17] than the average composite fracture toughness propagation $G_{Ii} = 599 \pm 37$ J/m^2.

At a first glance, there is no direct correspondence between the energy accumulation of the beam arms with a number of rows of tow that leads to unstable crack propagation.

Defects on the fabric surface, as voids or isles of matrix at the crack path, are accounted for in the variation of G_{Ii} for each coupon.[18] Another variation of the elastic energy accumulation depends on whether it is a T_{90° tows dominated area of $A_{T_{90^\circ}}/A_{T0^\circ} = 2.33$ or a T_{0° tows dominated area of $A_{T_{90^\circ}}/A_{T0^\circ} = 1.17$, both measured from split coupons as illustrated in Figure 1.

The values of G_{Ic} are summarized in Table 1. Note that G_{Ic} values are lower than the G_{Ii} values associated to propagation process. The lower G_{Ic} values are due to less interaction with the fabric surface at the crack tip.

Mode II – onset and propagation

The procedure to obtain G_{IIi} for propagation using the visual method for crack measurement is less accurate, sometimes impossible, and more difficult as compared to mode I using the same measuring device. This difficulty is due to the compressing load acting perpendicularly to the crack propagation direction, and

Table 1. Fracture toughness values of crack onset for mode I and respective critical load and displacement.

Coupon number	G_{IC} (J/m^2)	P_{IC} (N)	δ_{IC} (mm)
CP1	515	46.00	12.44
CP2	413	37.08	12.39
CP3	360	40.14	11.22
CP4	394	36.00	12.6
CP5	522	46.00	14.01
Average	441	41.04	13
STD	73	4.77	0.77
CV	16.70%	11.63%	6.00%

Note: CV: coefficient of variation; STD: standard deviation.

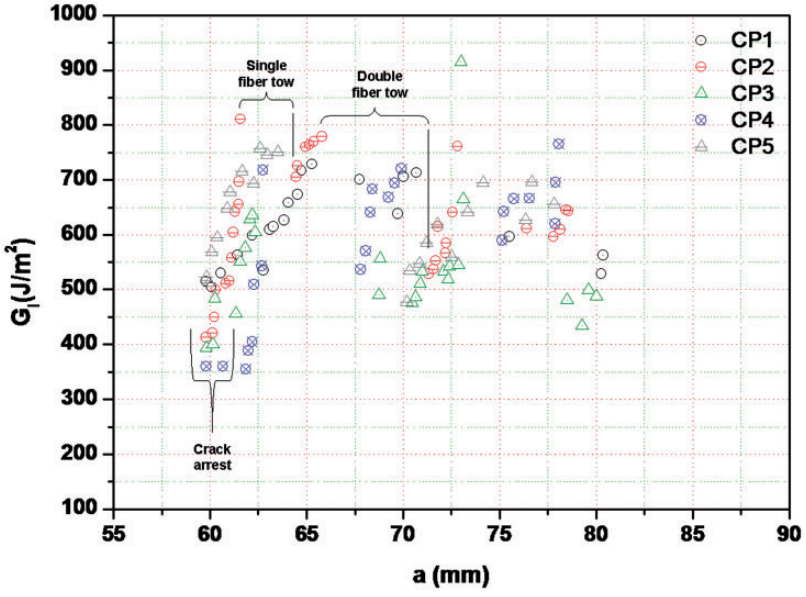

Figure 4. Crack propagation with decreasing G_i in mode I.

consequently closing it, thereby making it more difficult for visualization.

Another issue is the development of a fracture process zone ahead of the crack tip in this mode, in which crack measurement by visual procedure does not take into account the damage ahead the main crack,[19] which is not sharp as it occurs in mode I.

One way to avoid the crack length measurement is by using the crack equivalent method (a_e), that can be calculated using equation (1). The method is based on compliance-based beam method that depends on the corrected coupon compliance, obtained by equation (2). The equations and procedures are well outlined in work conducted by Moura et al.[19]

$$a_e = \left[\frac{C_{\text{corr}}}{C_{0\text{corr}}}a_0^3 + \frac{2}{3}\left(\frac{C_{\text{corr}}}{C_{0\text{corr}}} - 1\right)L^3\right]^{1/3} \quad (1)$$

$$C_{\text{corr}} = C - \frac{3L}{10G_{13}Bh} \quad (2)$$

In equations (1) and (2), the index 0 means the initial crack length, B is the coupon width, h is the half thickness of the coupon, and G_{13} is the shear modulus, in which was adopted a value of 4.3 GPa for this epoxy matrix system.

Then the value of $G_{\text{II}i}$ can be calculated with equation (3) using the flexural modulus obtained in equation (4), that is, a constant value for each coupon.

$$G_{\text{II}i} = \frac{9P^2a_e^2}{16B^2E_fh^3} \quad (3)$$

$$E_f = \frac{3a_0^3 + L^3}{8Bh^3C_{0\text{corr}}} \quad (4)$$

By comparing the crack development in Figure 5 with Figure 6, the reader may notice that a sharp crack tip itself did not exist but a damage zone that conducted multiple points of damage.

Within 2 mm of crack propagation that corresponds to a fiber tow, there is a smooth formation of the damage zone followed by an energy accumulation at the T_{90° row of tows, and simultaneously a formation of multiple points of damage far from the arresting point with small crack jump (one row of fiber tow), that can be seen in Figure 6.

For the first crack increments at the arresting point on the T_{90° tows, the crack changed the direction as a manner to overcome the barrier imposed by the T_{90° tows, and as a consequence, a few damages ahead of the arresting point were developed. As the crack developed in the damage zone, the propagation returned to the midplane at the end of the crack length. The whole process is exemplified in Figure 5.

The aforementioned description is summarized in the R-curve as shown in Figure 6, where the first point in each curve is the $G_{\text{II}c}$.

The fracture toughness in mode II was determined by NL methodology as there is a sharp change of the load–displacement linearity as the crack onset event takes place. Determining it visually is not as an easy task as conducted for mode I, as such event for mode II is just visually available after a few millimeters ahead of the precrack.

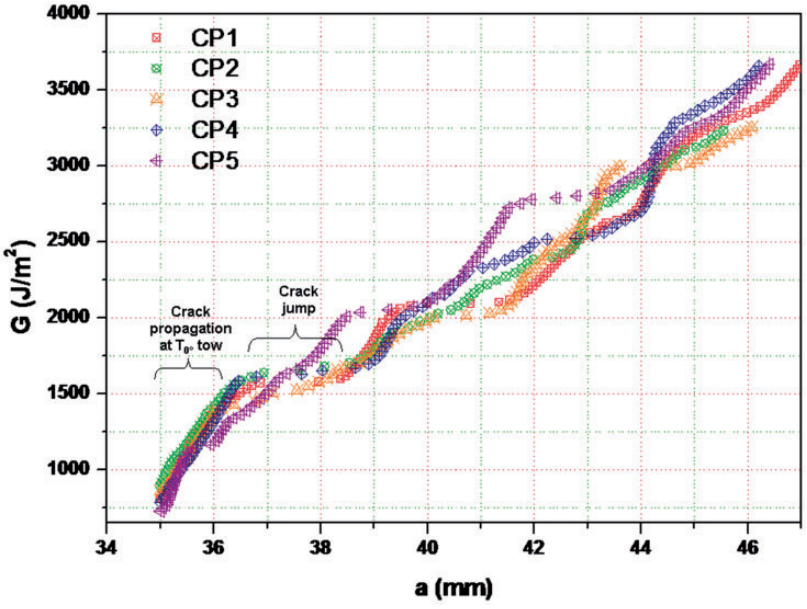

Figure 5. Crack propagation from the edge in mode II – coupon 4.

With the exception of CP5, all coupons had a similar slope in the R-curve that corresponded to a smooth crack growth, and for every 1.5 mm of plateau this event repeated until reaching 41 mm of the crack length.

From the analysis of CP4 images in Figure 6a, the first region is associated to stable crack growth at T_{0° tow between 35 and 36.5 mm of crack length as seen in Figure 5, when the energy increased linearly which gave a slope. This process was not detectable by visual technique, only the unstable propagation until 37 mm crack length the crack could be detected. The crack development at each row of tows that cannot be visually detected with magnified images was well predicted by crack equivalent method considered for the $G_{\mathrm{II}i}$ calculation, and by comparing a few measured cracks with the corresponding energy.

Regarding the anomalous behavior of CP5, the problem may be addressed to initial position of the insert film that drove the initial crack to a layer above the precrack plane, as seen in Figure 7. This characterized an asymmetric crack growth that showed different behavior from other curves of the delamination resistance curve.

Mollon et al.[20] reported a difference in $G_{\mathrm{I}c}$ of symmetric from asymmetric crack configuration based on the parabolic distribution of shear stress along the thickness, as described in equation (5). Therefore, the load increases as moving to a position above from the midplane.

$$\sigma_S = \frac{P}{2I}\left(h^2 - y^2\right) \tag{5}$$

where I is the inertia moment and y is the position along the thickness from the midplane.

By comparing symmetric and asymmetric crack configuration in Figures 6 and 7, respectively, it is possible to visualize more ply separation at the midplane, for the same crack length measurements, in the first case, hence indicating more contribution of mode I.

In accordance with ASTM D 6671/D 6671 M-06[21] for mixed mode test, the maximum crack length must be equal to $a_m = L - 3h$, which in these tests corresponded to 44.9 mm length or the last crack jump that occurred in all coupons (with an initial jump at ≈ 41 mm and ending up in ≈ 46 mm). After 44.9 mm of crack length, the crack has an influence of the loading nose according to the test procedure.

Based on the crack mechanism given in literature[22,23] and the fracture damage zone phenomena, it is possible to explain the lack of energy decreasing in $G_{\mathrm{II}i}$ versus a that mode I presented in its R-curves, which is regarded as steady-state plateau or propagation toughness. As a series of micro-tensile acts in the cusps formation and try to overcome the T_{90° row of tows, in the meanwhile,

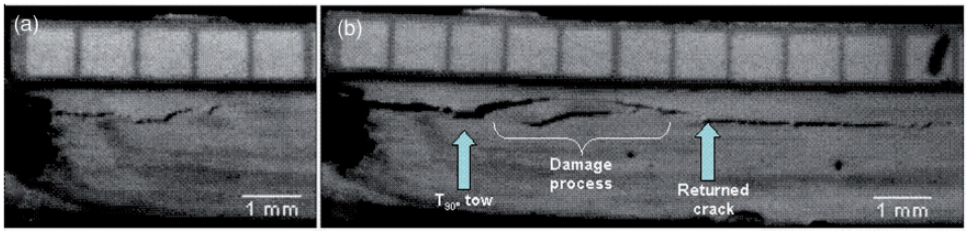

Figure 6. Crack propagation in mode II for coupons 1–5.

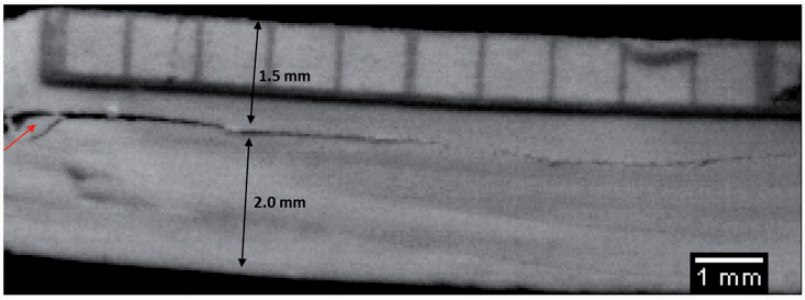

Figure 7. Asymmetric crack propagation in mode II for coupon 5.

Table 2. Fracture toughness values of crack onset for mode II and respective critical load and displacement.

Coupon number	G_{IIC} (J/m^2)	F_{IIC} (N)	δ_{IIC} (mm)
1	891	445.03	3.47
2	860	433.67	3.44
3	814	428.14	3.30
4	785	420.49	3.24
5	726	403,65	3.12
Average	815	426.20	3.31
STD	65	15.45	0.14
CV	7.91%	3.63%	4.36%

Note: CV: coefficient of variation; STD: standard deviation.

another series of micro-tensile had already been formed ahead of the crack tip, but in smaller size. As soon as the fracture occurs at the first series of cusps, there are another T_{90° row of tows holding the next formation thereafter stabilizing the energy for each interaction. The continuous raising in G_{IIi} might be understood as an increase of surface extension in which cusp formation mechanisms acts with further crack progression.

The singular point at $\approx$41 mm of crack length represents the maximum extension of the delamination process regarding pure mode II, where a crack jump occurred for all coupons. From this point, there is an increase in asymmetric deformation from the loading nose that implies in the out-of-plane loads. The fracture in this area may be dominated by cleavage associated to mode I contribution.

Table 2 summarizes the results of the tests.

The NL event for mode II fracture toughness can be considered a more appropriate method to detect minor changes in the matrix integrity as the visual technique used for mode I is not able to show these minor changes. The adopted approach reflected in low value of CV of 7.91%.

Conclusions and final remarks

The crack propagation behavior in quasi static load through a nonplanar surface was explained in this research based on the energy concept for modes I and II opening. The validation of the standard ASTM D5528-01 could be extended for this material as G_{Ic} showed similar CV found for unidirectional composites when it is determined by visual identification of the crack onset. Regarding the condition (crack tip pointed toward a plane above the midplane), the crack tip is constrained by fabric waviness during the manufacturing process, it was also considered in CV variation.

The R-curve of such structure is comparable with the bridging effect found in unidirectional laminates, which is related to interference in ASTM D5528-01; therefore, it also has its applicability based on a systematic crack increment drove by the surface pattern.

Even though a standard test method for mode II is still under development,[14,24] G_{IIc} presented low CV that may indicate a well-adopted procedure. For G_{IIi} energy propagation, it may need more adjustments to indicate a defined delamination resistance plateau that could be achieved by increasing the span length to evaluate further propagation. The downside of mode II fracture toughness is the lack of visual technique for crack measurement because of the fracture process zone that limits an accurate evaluation.

Funding

Financial support was received from FAPESP, contract numbers 2012/07646-0 and 2011/01937-0.

Conflict of interest

None declared.

References

1. Stelzer S, Brunner AJ, Arguelles A, et al. Mode I delamination crack growth in unidirectional fiber reinforced composites: development of standardized test procedure. *Comp Sci Tec* 2012; 72: 1102–1107.
2. Kenane M and Benmedakhene S. Fracture and fatigue of unidirectional glass/epoxy laminate under mode of loading. *Fatigue Fract Eng Mater Struct* 2010; 33: 284–293.
3. Gong KJ, Hurez A and Verchery G. On the determination of delamination toughness by using multidirectional DCB specimens. *Polym Test* 2010; 29: 658–666.
4. Todo M and Jar P-YB. Study of mode-I interlaminar crack growth in DCB specimens of fibre-reinforced composites. *Compos Sci Technol* 1998; 58: 105–118.
5. Martin RH. Interlaminar fracture characterization. *Key Eng Mater* 1996; 120–121: 329–346.
6. Ebeling T, Hiltner A and Baer E. Delamination failure of a woven glass fiber composites. *J Compos Mater* 1997; 31: 1318–1333.
7. Alif N, Carlsson LA and Boogh L. The effect of weave pattern and crack propagation direction on mode I delamination resistance of woven and carbon composites. *Compos B* 1998; 28B: 603–611.
8. Gill AF, Robinson P and Pinho S. Effect of variation in fibre volume fraction on modes I and II delamination behavior of 5HS woven composites manufactured by RTM. *Compos Sci Technol* 2009; 69: 2368–2375.
9. Hadavinia H and Ghasemnejad H. Effects of mode-I and mode-II interlaminar fracture toughness on the energy absorption of CFRP twill/weave composite box sections. *Compos Struct* 2009; 89: 303–314.
10. De Baere I, Jacques S, Van Paepegem W, et al. Study of the mode I and Mode II interlaminar behaviour of

carbon fabric reinforced thermoplastic. *Polym Test* 2012; 31: 322–332.
11. Schuecker C and Davidson BD. Evaluation of the accuracy of the four-point bend end-notched flexure test for mode II delamination toughness determination. *Compos Sci Technol* 2000; 60: 2137–2146.
12. ASTM D 5528-01 (Reapproved 2007). Standard Test Method for Mode I Interlaminar Fracture Toughness of Unidirectional Fiber-Reinforced Polymer Matrix Composites. In: *Annual book of ASTM Standards*. Vol. 15.03, Philadelphia: American Society for Testing and Materials, 2008.
13. Argüeles A, Vina J, Canteli AF, et al. Fatigue delamination, initiation, and growth, under mode I and II of fracture in a carbon-fiber epoxy composites. *Polym Compos* 2010; XX: 701–708.
14. O'Brien TK, Johnston WM and Toland GJ. Mode II interlaminar fracture toughness and fatigue characterization of a graphite epoxy composite material. Report/Patent number: *NASA/TM* 2010-216838.
15. ASTM D6856/D6856M-03(2008)e1. *Standard guide for testing fabric-reinforced ''textile'' composite materials*. In: *Annual book of ASTM Standards*. Vol. 15.03, Philadelphia: American Society for Testing and Materials, 2008.
16. La Saponara V and Kardomateas GA. Crack branching in cross-ply composites: an experimental study. *Compos Struct* 2001; 53: 333–344.
17. HEXFLOW®RTM6-2. Product Data. Publication ITA Dublin, California 2010.
18. Costa AL, Almeida SF and Rezende MC. Resistencia ao cisalhamento interlaminar de compositos com resina epoxi com diferentes arranjos das fibras na presenca de vazios. *Polimeros* 2001; 11: 182–189.
19. Moura MFSF, Campilho RDSG and Goncalvez JPM. Pure mode II fracture characterization of composite bonded joints. *Int J Solids Struct* 2009; 46: 1589–1595.
20. Mollon V, Bonhomme J, Arguelles A, et al. Influence of the crack plane over GII results in carbon epoxy ENF specimens. *Compos Struct* 2012; 94: 1187–1191.
21. ASTM D 6671/D 6671M-06. Standard test method for mixed mode I–mode II interlaminar fracture toughness of unidirectional fiber reinforced polymer matrix composites. In: *Annual book of ASTM Standards*. Vol. 15.03, Philadelphia: American Society for Testing and Materials, 2006.
22. Purslow D. Matrix fractography of fibre-reinforced epoxy composites. *Composites* 1986; 17: 289–294.
23. Greenhalgh ES, Rogers C and Robinson P. Fractographic observations on delamination growth and subsequent migration through the laminate. *Compos Sci Technol* 2009; 69: 2345–2351.
24. O'Brien TK. Interlaminar fracture toughness: the long and winding road to standardization. *Compos B* 1998; 29B: 57–62.